Supporting Information

Song et al. 10.1073/pnas.1013377108

SI Text

Preparation of Uniformly ^{13}C- and ^{15}N-Labeled Phycocyanobilin (PCB) Chromophore (*u*-[^{13}C,^{15}N]-PCB). Axenic cultures of *Synechocystis* 6803 were cultivated in 500 mL sterile-filtered BG11 medium including 60 mM CHAPS pH 8.0, $Na^{15}NO_3$, and $NaH^{13}CO_3$ (1) in 1-L bottles under continuous white light at a fluence rate of 30 $\mu mol \cdot m^{-2} \cdot s^{-1}$ photosynthetically active radiation on rotary shakers at 26 °C. Typically, approximately 10 L stationary phase ($OD_{750} \sim 3$, after about 6–8 wk growth) culture was pelleted, washed, and resuspended in cold 100 mM K_2HPO_4 buffer (pH 7.0), 5 mM EDTA, and lysed by three passes through a French pressure cell at 7 MPa. The supernatant was clarified and precipitated with 0.7 vol 3.3 M ammonium sulfate, 50 mM Tris, 1 mM imidodiacetic acid (IDA) (pH 7.8). Working in subdued light, the deep-blue precipitate was pelleted and washed with cold methanol until the supernatant was essentially clear and colorless. The pellet was finally resuspended in 200 mL methanol and subjected to methanolysis in darkness at 54 °C overnight with stirring. The crude PCB extract was clarified and the supernatant concentrated in a rotary evaporator, 1 vol H_2O added and prepurified via reverse-phase C18 cartridges (Sep-Pak Plus, Waters), eluting with methanol. This procedure was followed by isocratic HPLC purification using an UltraSep ES PHARM RP18E preparative column (SepServ, 250 × 20 mm, particle diameter 7 μm) with a 60 × 20 mm precolumn at a flow rate of 6 mL/min and 4.2 MPa with 70% 7.5 mM NaHPO4 (pH 6.0) and 30% acetonitrile running buffer. After HPLC, the solvent was exchanged via a C18 cartridge into methanol allowing the *u*-[^{13}C,^{15}N]-PCB to be concentrated to approximately 1 mM by evaporation. Aliquots (500 nmol) were stored in darkness at −80 °C.

Preparation of *u*-[^{13}C,^{15}N]-PCB-Cph1Δ2 (Residues 1–514 of Cph1 Phytochrome with an Additional C-terminal His_6-Tag) as Pr and Pfr. For Cph1Δ2 apoprotein production, BL21 Pro chemically competent *Escherichia coli* cells were cotransformed with plasmids p926.5 and pSE111 (1). Cells were grown at 37 °C to $OD_{600} = 0.4$, chilled, and overnight expression induced with 20 μM IPTG at 18 °C. The cells were pelleted, washed, and lysed in a French pressure cell in TESβ buffer (50 mM Tris, 5 mM EDTA, 300 mM NaCl, 1 mM β-mercaptoethanol, pH 7.8) at 7 MPa. The clarified supernatant was precipitated with 0.7 vol of 3.3 M ammonium sulfate containing 50 mM Tris, 1 mM IDA, pH 7.8. The precipitate was dissolved in $TISI^{10}$ (50 mM Tris/Cl, 1 mM IDA, 300 mM NaCl, 10 mM imidazole, 1 mM β-mercaptoethanol, pH 7.8) and clarified. The apoprotein was purified by nickel affinity chromatography (Qiagen Ni-NTA Superflow; 60 × 10 mm) with a flow rate of 1 mL/min on an automated FPLC apparatus (ÄKTA, Pharmacia/GE). The apoprotein was eluted in $TISI^{100}$ (50 mM Tris/Cl, 1 mM IDA, 300 mM NaCl, 100 mM imidazole, 1 mM β-mercaptoethanol, pH 7.8) and was again precipitated and dissolved in TESβ for assembly with a 10% excess of *u*-[^{13}C,^{15}N]-PCB in darkness overnight at 4 °C.

Pr and Pfr holoprotein was prepared by saturating irradiation followed by preparative size exclusion chromatography (HiLoad 26/60 Superdex 200 prep grade, Pharmacia/GE) at 2 mL/min and finally concentrated by ultrafiltration using an Amicon Stirred Cell (Millipore) followed by Vivaspin 500 tubes (Vivascience). All procedures were carried out in total darkness using infrared visualization with a CCD camera and head-mounted goggles (Trivisio).

Pr holoprotein was prepared as follows: Twenty-five milligrams holoprotein at 5 mg/mL was photoconverted to Pr by saturating irradiation in a 250 μL Hamilton syringe with far-red light from an array of 730 nm (20 nm FWHM) light-emitting diodes (LEDs) and loaded onto the column via a sample loop. The eluted Pr monitored at 660 nm was pooled as a 90% cut.

Pfr holoprotein was prepared as follows: Although only 70% Pfr is formed at photoequilibrium in red light, it proved possible to prepare Pfr at near 100% occupancy by exploiting its higher propensity to dimerise relative to Pr (2). After saturating irradiation with red light from 660 nm (20 nm FWHM) LEDs as above, 15 mg protein at 3 mg/mL was loaded onto the column. Pfr dimers monitored at 700 nm were pooled from the fractions up to 0.5 mL before the peak was reached, thereby excluding monomeric Pr which began to elute at this point.

Resonance Assignments of MELODI–HETCOR NMR Spectra for Cph1Δ2 as Pr and Pfr. Our previous 2D homonuclear ^{13}C–^{13}C dipolar-assisted rotational resonance (DARR) NMR studies on various states of Cph1Δ2 and *phyA*65 containing *u*-[^{13}C,^{15}N]-PCB chromophore provide full sets of ^{13}C chemical shifts (3, 4) and hence the basis for the interpretation of the intermolecular ^{1}H–^{13}C spectra presented in Figs. S1 and S2. The ^{13}C chemical shifts in the present study (summarized in Dataset S3) are well in line with the values reported ($\Delta\sigma^C \leq 0.2$ ppm), except for the C16 resonance as Pfr exhibiting a 0.5-ppm up-field shift, the origin of which is not clear. These two heteronuclear spectra were recorded with a 2.3-ms Lee–Goldburg cross-polarization contact time, which was sufficiently long to detect the interfacial ^{1}H correlations of the chromophore up to approximately 4.5 Å. However, the cutoff distance used to define the potential ^{1}H–^{13}C correlations was set to 5.5 Å due to the thermal motion of protein atoms on the timescale of picoseconds, expressed as rms fluctuations (approximately 0.5 Å for each atom) (5). The Cph1 Pr 2VEA 3D sensory module structure of the Pr state (in the *ZZZssa* geometry) (6) provides a reliable template for assigning the intermolecular ^{1}H–^{13}C correlation signals presented in Fig. S1. For each chromophore carbon, we measured all possible intermolecular residue contacts within enclosure sphere up to approximately 5.5 Å. For example, ring ***D*** forms a strong hydrogen bond via its carbonyl group (C19, 173.7 ppm in the ω_2-dimension) with the imidazole moiety of the highly conserved His-290 (an O···Nϵ2 distance of 2.80 Å) (6). The buildup kinetics of a long-range intermolecular correlation primarily depends on the heteronuclear distance (7–9). Thus, the cross-peak intensities can provide a fair estimation of the ^{1}H–^{13}C proximities. Therefore, we assign this interaction (His-290 $H^{N\epsilon 2}$···C19) to the most intense cross-peak centered at 12.7 ppm in the down-field ^{1}H frequencies of 10–13 ppm (Fig. S1), which is further confirmed by ^{1}H correlations with the adjacent carbons of the C19, e.g., His-290 $H^{N\epsilon 2}$···C18 having a crystal distance of 4.60 Å, and with the ethyl side chain, $C18^1$ (5.10 Å) and $C18^2$ (4.29 Å) of ring ***D***, locating at 134.2, 16.5, and 13.2 ppm in the ω_2-dimension, respectively (Fig. S1 and Dataset S4). In contrast, the correlation signal of His-290 $H^{N\epsilon 2}$···C17 is not completely resolved because they are 5.47 Å apart in the Cph1 crystal structure (6), close to the limit of the transfer range. Approximately 60% Pr correlations can match the intermolecular distance constraints extracted from the 2VEA Pr X-ray diffraction structure (Dataset S3). Part of the long-range heteronuclear correlations involving transfer of ^{1}H polarization from methine groups (i.e., H^{α}, H^{ζ}, etc.) to carbonyls (C1 and C19) and pyrrolic quaternary carbons (C4 and C6) as well as 10/15-methine carbons and rapidly rotating methyls ($C7^1$, $C17^1$, and $C18^2$) are evidently not resolved. This effect re-

sults from the truncation of weak long-range heteronuclear dipolar interactions by strong one-bond heteronuclear couplings (9–12). Despite REDOR (rotational echo double-resonance) dipolar-filtering approach employed in the MELODI–HETCOR (medium- and long-distance heteronuclear correlation) method (7, 8), both weak and strong heteronuclear dipolar couplings are still present in the Hamiltonian of the ^{1}H spins, and thus the weak couplings are truncated. In contrast, some protons in protonated ammonium and methyl groups of nearby amino acids are found to transfer magnetization over relatively long distances, for example, Tyr-257 $H^{N}\cdots C8^{1}$, 4.93 Å; Ile-208 $H^{N}\cdots$C15, 4.95 Å; Leu-15 $H^{C\delta 2}\cdots$C2, 4.80 Å; and Met-174 $H^{C\epsilon}\cdots$C18, 4.65 Å (Dataset S4). Similarly, the polarization transfers from protons of the methylene groups in the mode of a ^{13}C–$^{13}CH_2$ moiety to remote carbons are detected (e.g., Ile-208 $H^{C\beta}\cdots$C13, 4.88 Å) (13). Due to weakness of the signal, the C5-methine carbon originally appearing at approximately 87.1 ppm (3) is not resolved in the ω_2-dimension.

In addition, the PaBphP Pfr 3C2W structure (14) is helpful in recognizing potential ^{1}H contacts around the chromophore (within an enclosure sphere up to approximately 5.5 Å) for pure Cph1Δ2 Pfr (Fig. S2). A comparison between 2VEA and 3C2W revealed both structural similarities and differences within the PCB-binding pocket upon photoconversion as reviewed in Hughes (15) and in Rockwell and Lagarias (16). More specifically, 3C2W shows a different chromophore attachment site of ring ***A*** and tautomeric differences of several tyrosine side chains surrounding ring ***D*** (for example, Tyr-163 and Tyr-190, PaBphP numbering), none of which are particularly surprising. However, most of conserved residues within approximately 5.5 Å of the Pr-state PCB chromophore do not exhibit significantly different positions from those in 3C2W; for example, the highly conserved Asp-194 (PaBphP numbering, equivalent to Asp-207 in Cph1) and His-247 (His-260 in Cph1) in close proximity to the chromophore (lying on the β- and α-face of the chromophore ring system, respectively). The 3C2W sequence for the core region of the GAF (cGMP phosphodiesterase adenylyl cyclase/FhlA) domain (residue range of 157–280) is approximately 50% identical (66/124) to that in 2VEA (residue range of 170–293) and particularly 17 out of a total of 23 residues detected in the Pr state (Fig. 1*B*) are well conserved in 3C2W Pfr sequence, as compared in Dataset S5.

1. Strauss HM, Hughes J, Schmieder P (2005) Heteronuclear solution-state NMR studies of the chromophore in cyanobacterial phytochrome Cph1. *Biochemistry* 44:8244–8250.
2. Strauss HM, Schmieder P, Hughes J (2005) Light-dependent dimerisation in the N-terminal sensory module of cyanobacterial phytochrome 1. *FEBS Lett* 579:3970–3974.
3. Rohmer T, et al. (2008) Light-induced chromophore activity and signal transduction in phytochromes observed by ^{13}C and ^{15}N magic-angle spinning NMR. *Proc Natl Acad Sci USA* 105:15229–15234.
4. Rohmer T, et al. (2010) Phytochrome as molecular machine: Revealing chromophore action during the Pfr → Pr photoconversion by magic-angle spinning NMR spectroscopy. *J Am Chem Soc* 132:4431–4437.
5. Treutlein H, et al. (1992) Chromophore–protein interactions and the function of the photosynthetic reaction center: A molecular dynamics study. *Proc Natl Acad Sci USA* 84:75–79.
6. Essen L-O, Mailliet J, Hughes J (2008) The structure of a complete phytochrome sensory module in the Pr ground state. *Proc Natl Acad Sci USA* 105:14709–14714.
7. Yao XL, Schmidt-Rohr K, Hong M (2001) Medium- and long-distance ^{1}H–^{13}C heteronuclear correlation NMR in solids. *J Magn Reson* 149:139–143.
8. Yao XL, Hong M (2001) Dipolar filtered ^{1}H–^{13}C heteronuclear correlation spectroscopy for resonance assignment of proteins. *J Biomol NMR* 20:263–274.
9. van Rossum B-J, de Groot CP, Ladizhansky V, Vega S, de Groot HJM (2000) A method for measuring heteronuclear (^{1}H–^{13}C) distances in high speed MAS NMR. *J Am Chem Soc* 122:3465–3472.
10. Brus J, Jegorov A (2004) Through-bonds and through-space solid-state NMR correlations at natural isotopic abundance: Signal assignment and structural study of simvastatin. *J Phys Chem A* 108:3955–3964.
11. Bayro MJ, et al. (2009) Dipolar truncation in magic-angle spinning NMR recoupling experiments. *J Chem Phys* 130:114506.
12. Ladizhansky V, Vinogradov E, van Rossum B-J, de Groot HJM, Vega S (2003) Multiple-spin effects in fast magic angle spinning Lee–Goldburg cross-polarization experiments in uniformly labeled compounds. *J Chem Phys* 118:5547–5557.
13. Ladizhansky V (2009) Homonuclear dipolar recoupling techniques for structure determination in uniformly ^{13}C-labeled proteins. *Solid State Nucl Magn Reson* 36:119–128.
14. Yang X, Kuk J, Moffat K (2008) Crystal structure of *Pseudomonas aeruginosa* bacteriophytochrome: Photoconversion and signal transduction. *Proc Natl Acad Sci USA* 105:14715–14720.
15. Hughes J (2010) Phytochrome three-dimensional structures and functions. *Biochem Soc Trans* 38:710–716.
16. Rockwell NC, Lagarias JC (2010) A brief history of phytochromes. *ChemPhysChem* 11:1172–1182.

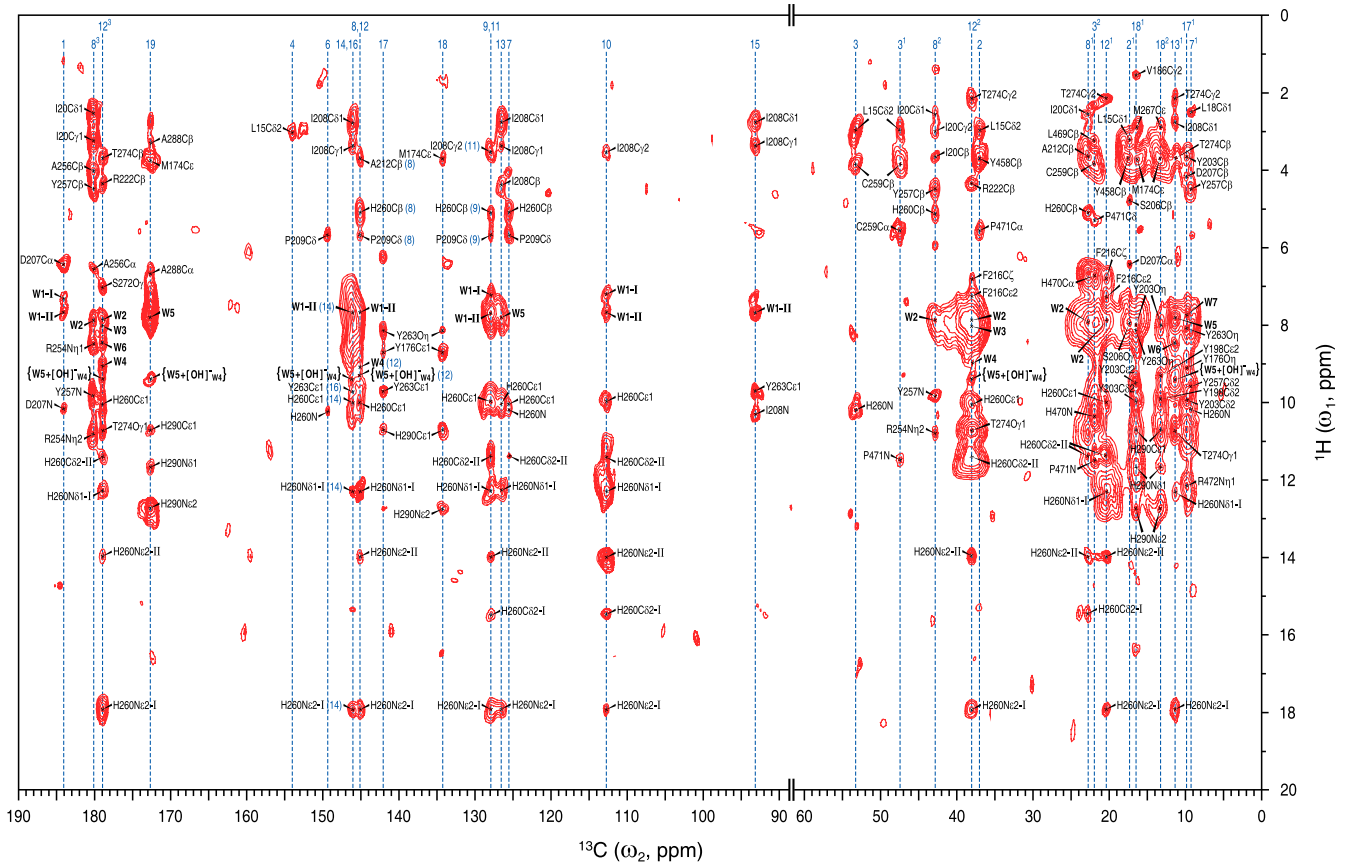

Fig. S1. Solid-state magic-angle spinning (MAS) NMR spectrum of *Synechocystis* Cph1Δ2 in the Pr state. Two-dimensional ^{1}H–^{13}C interfacial correlation spectrum from *u*-[^{13}C,^{15}N]-PCB-Cph1Δ2 with a Lee–Goldburg cross-polarization (LG–CP) contact time of 2.3 ms. The resolved chromophore correlations are solely due to the interactions with protons bound to the amino acids in its vicinity. Corresponding spectra of Cph1Δ2 at natural abundance and the intramolecular H^N contacts of the chromophore (with an LG–CP contact time of 900 μs) have been subtracted. The spectral region without resonances, 60–90 ppm (in ω_2-dimension), is omitted from the spectrum and ^{13}C resonances of the chromophore are labeled (on top of the dashed vertical lines) according to our previous 2D ^{13}C–^{13}C DARR NMR studies on this protein (3, 4). The notation for assignment uses Cph1 numbering of residues (6), followed by the Greek letter referring to the proton identity.

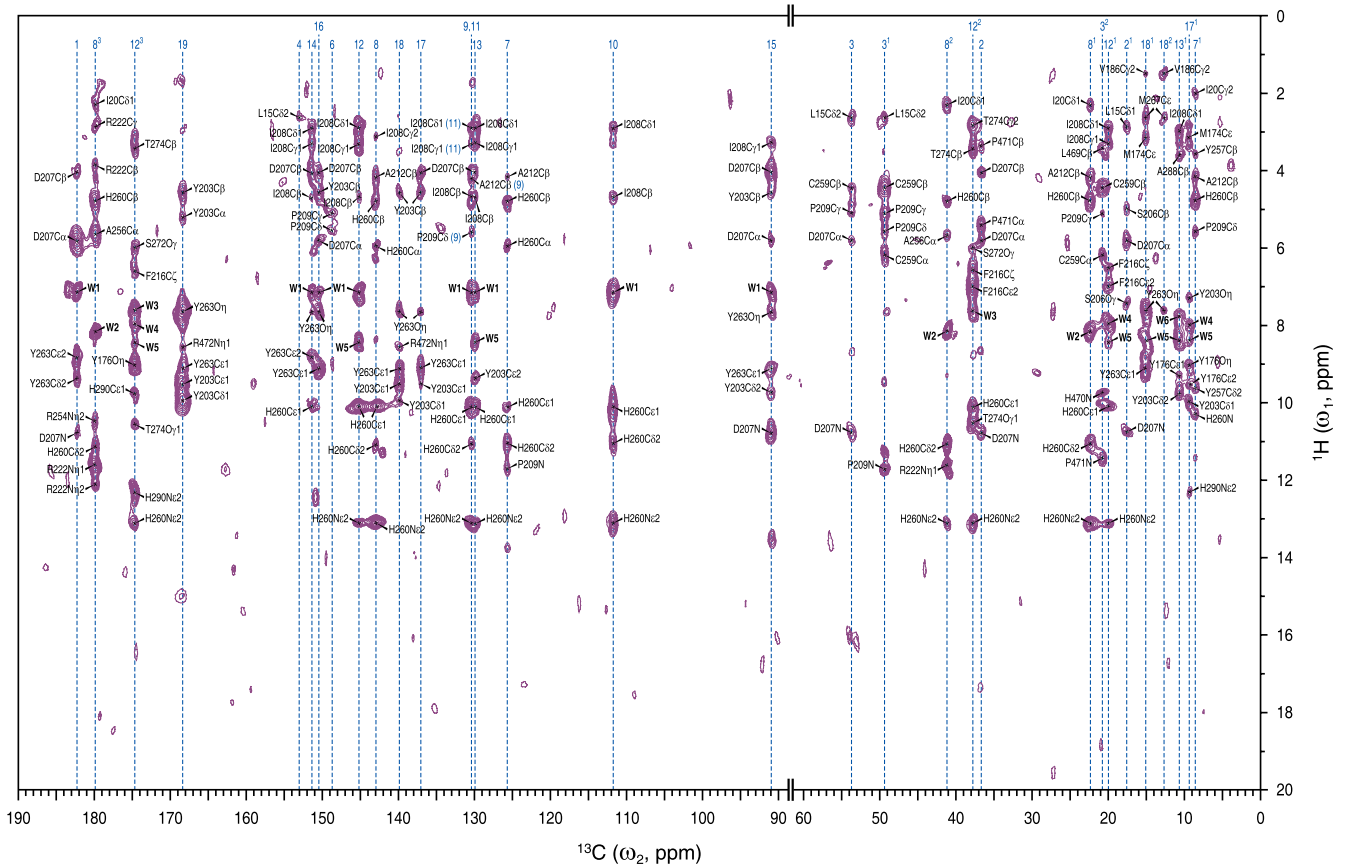

Fig. S2. Solid-state MAS NMR spectrum of *Synechocystis* Cph1Δ2 in the Pfr state. Two-dimensional ^{1}H–^{13}C interfacial correlation spectrum from *u*-[^{13}C,^{15}N]-PCB-Cph1Δ2 with a Lee–Goldburg cross-polarization (LG–CP) contact time of 2.3 ms. The resolved chromophore correlations are solely due to the interactions with protons bound to the amino acids in its vicinity. Corresponding spectra of Cph1Δ2 at natural abundance and the intramolecular H^N contacts of the chromophore (with an LG–CP contact time of 900 μs) have been subtracted. The spectral region without resonances, 60–90 ppm (in ω_2-dimension), is omitted from the spectrum and ^{13}C resonances of the chromophore are labeled (on top of the dashed vertical lines) according to our previous 2D ^{13}C–^{13}C DARR NMR studies on this protein (3, 4). The notation for assignment uses Cph1 numbering of residues (6), followed by the Greek letter referring to the proton identity.

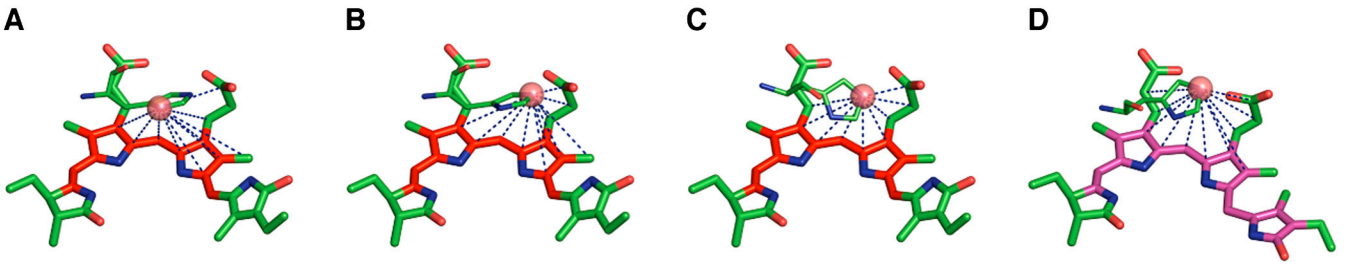

Fig. S3. Mobility of conserved His-260 inside the PCB-binding pocket. Long-range intermolecular ^{1}H–^{13}C correlations (indicated by black dashed lines) involving the proton attached to Nδ1/Nε2 in the cationic/neutral imidazole side chain of His-260, for Nδ1 (*A*) and Nε2 (*B*) in the cationic imidazole as **Pr-I**, Nε2 (*C*) in the neutral form as **Pr-II**, and Nε2 (*D*) as Pfr (for more details, see Dataset S4). The conjugation pattern of the PCB chromophore is colored in red for Pr (*A*–*C*) and purple for Pfr (*D*) (3).

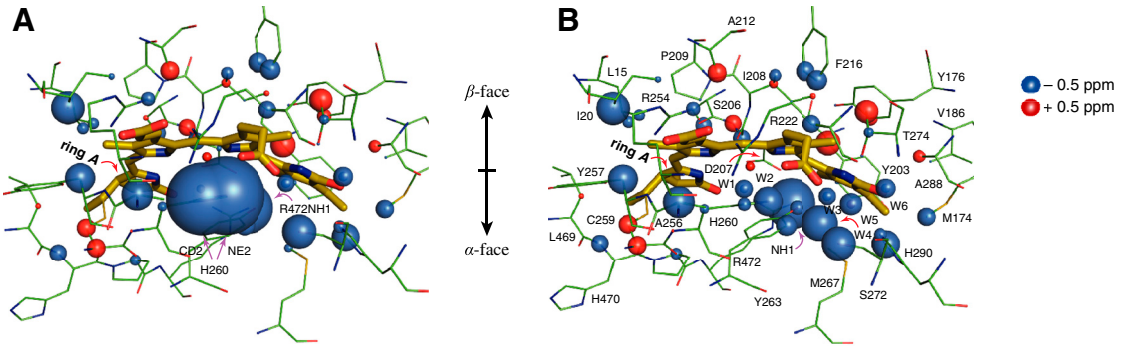

Fig. S4. Light-driven ^{1}H NMR chemical shift changes for amino acids surrounding the PCB chromophore. Side views of the observed chromophore ^{1}H contacts (shown in Figs. S1 and S2) highlight their chemical shift differences ($\Delta\sigma^H$) during Pr → Pfr photoisomerization (listed in Datasets S3 and S4). (*A*) **Pr-I** vs. Pfr, and (*B*) **Pr-II** vs. Pfr. The size of the red and blue spheres represents a Pfr minus Pr $\Delta\sigma^H$ of 0.1 ppm as PyMOL vdw parameter 0.2. For the sake of clarity, however, spheres for the protons attached to Nη1 of Arg-472 (*A* and *B*), and Nε2/Nδ1 of His-260 (*B*) are scaled by a factor of 0.5. Red and blue spheres represent down- and up-field shifts, respectively. Amino acids lying on the α-face of the coplanar ***B*** and ***C*** rings (indicated by the downward arrow, also see ref. 1) exhibit coherent up-field shifts (blue spheres), implying an overall more-shielded protein environment on photoconversion to Pfr, whereas the electronic surrounding of the β-face of the bilin ring system (indicated by the upward arrow) is diversely affected.

1 Rockwell NC, Shang L, Martin SS, Lagarias JC (2009) Distinct classes of red/far-red photochemistry within the phytochrome superfamily. *Proc Natl Acad Sci USA* 106:6123–6127.

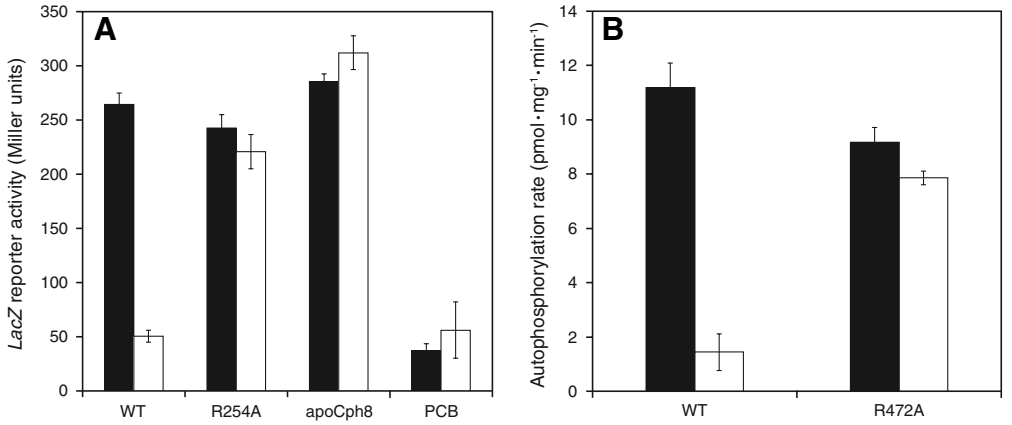

Fig. S5. Light-regulated signaling via the Arg-254/***B***-ring propionate and Asp-207/Arg-472 salt bridges. (*A*) In vivo signaling via the Arg-254/***B***-ring propionate salt bridge monitored genetically via a β-Galactosidase reporter Cph8 (1), a Cph1:EnvZ hybrid protein, was produced in RU1012 *E. coli* as a holoprotein by coexpression of the chimeric gene and pPL-PCB. The EnvZ phosphotransfer signal was read out from the *ompC*-driven β-Galactosidase by Miller assays performed 4 h after Cph8 induction at 30 °C under continuous far-red (735 nm; black bars) or red (660 nm; white bars) light. β-Galactosidase activity with either wild-type Cph8 (WT), R254A-Cph8 (R254A) holoprotein, apoCph8 (apoCph8), or only the chromophore (PCB). Miller assays were performed essentially as described (2). HoloCph8 is active as Pr (in far-red light) but displays a fivefold lower activity in red light. In contrast, the R254A-Cph8 mutant is constitutively active although the spectral behavior of the mutant is similar to that of the WT holoprotein (3). ApoCph8 too is constitutively active, in accordance with Levskaya et al. (1). Data represent the mean values of triplicate measurements with the standard deviations indicated. The RU1012 *E. coli* strain (4) and pPL-PCB (5) were kindly provided by R. E. Inouye and J. C. Lagarias, respectively. (*B*) In vitro signaling via the Asp-207/Arg-472 salt bridge monitored by autophosphorylation. Initial reaction rates for the autophosphorylation activity of purified WT- and R254A-Cph1 full-length holoproteins after saturating far-red (735 nm, black bars) or red (660 nm, white bars) irradiation and the addition of 33 μM ATP containing [γ-^{32}P]ATP. Reactions were carried out in darkness, 10 μL aliquots being removed under dim blue-green safelight (495 nm) at desired time points. Sample reactions were stopped in SDS sample buffer, run out on SDS-PAGE, and activity measured by a PhosphorImager (Fuji, FLA-7000). Initial reaction rates were determined within the linear period of the reaction using GraphPad Prism software. Strong autophosphorylation of Pr is observed for both WT- and R472A-Cph1 holoproteins. Wild-type autophosphorylation is greatly reduced following red irradiation, however, in accord with Yeh et al. (6). In the case of R472A, however, autophosphorylation is similar to wild-type Pr regardless of the preirradiation, although the spectral behavior of the mutant is similar to that of the WT holoprotein (3). Data correspond to kinetic measurements in triplicate, the bars denoting standard deviation.

1 Levskaya A, et al. (2005) Synthetic biology: Engineering *Escherichia coli* to see light. *Nature* 438:441–442.
2 Miller JH (1972) Experiments in molecular genetics (Cold Spring Harbor Laboratory Press, New York).
3 Essen L-O, Mailliet J, Hughes J (2008) The structure of a complete phytochrome sensory module in the Pr ground state. *Proc Natl Acad Sci USA* 105:14709–14714.
4 Gambetta GA, Lagarias JC (2001) Genetic engineering of phytochrome biosynthesis in bacteria. *Proc Natl Acad Sci USA* 98:10566–10571.
5 Utsumi R, et al. (1989) Activation of bacterial porin gene expression by a chimeric signal transducer in response to aspartate. *Science* 245:1246–1249.
6 Yeh K-C, Wu S-H, Murphy JT, Lagarias JC (1997) A cyanobacterial phytochrome two-component light sensory system. *Science* 277:1505–1508.

Other Supporting information Files

Dataset S1 (PDF)
Dataset S2 (PDF)
Dataset S3 (PDF)
Dataset S4 (PDF)
Dataset S5 (PDF)